PROCEEDINGS OF SCIENCE

Pion polarizability from four-point functions in lattice QCD

Frank X. Lee,[a] **Andrei Alexandru,**[a] **Chris Culver**[b] **and Walter Wilcox**[c]

[a] *Physics Department, The George Washington University, Washington, DC 20052, USA*
[b] *Department of Mathematical Sciences, University of Liverpool, Liverpool L69 7ZL, United Kingdom*
[c] *Department of Physics, Baylor University,Waco, Texas 76798, USA*
E-mail: fxlee@gwu.edu, aalexan@gwu.edu, c.culver@liverpool.ac.uk, walter_wilcox@baylor.edu

Polarizabilities reveal valuable information on the internal structure of hadrons in terms of charge and current distributions. For neutral hadrons, the standard approach is the background field method. But for a charged hadron, its acceleration under the applied field complicates the isolation of the polarization energy. In this work, we explore an alternative method based on four-point functions in lattice QCD. The approach offers a transparent picture on how polarizabilities arise from quark and gluon interactions. We carry out a proof-of-concept simulation on the electric polarizability of a charged pion, using quenched Wilson action on a $24^3 \times 48$ lattice at $\beta = 6.0$ with pion mass from 1100 to 370 MeV. We report results on charge radius and electric polarizability. Our results from connected diagrams suggest that charged pion α_E is due to a large cancellation between elastic and inelastic contributions, leaving a small and positive value that has a relatively mild pion mass dependence.

The 39th International Symposium on Lattice Field Theory, LATTICE2022, 8-13 August, 2022, Bonn, Germany

PoS(LATTICE2022)115

1. Introduction

Understanding electromagnetic polarizabilities has been a long-term goal of lattice QCD. The challenge in the effort lies in the need to apply both QCD and QED principles. The standard approach to compute polarizabilities is the background field method which has been widely used for dipole polarizabilities. Methods to study higher-order polarizabilities have also been proposedin this approach. Although such calculations are relatively straightforward, requiring only energy shifts from two-point functions, there are a number of unique challenges. First, since weak fields are needed, the energy shift involved is very small relative to the mass of the hadron (on the order of one part in a million depending on the field strength). This challenge has been successfully overcome by relying on statistical correlations with or without the field. Second, there is the issue of discontinuities across the boundaries when applying a uniform field on a periodic lattice. This has been largely resolved by using quantized values for the fields, or Dirichlet boundary conditions. Third and more importantly, a charged hadron accelerates in an electric field and exhibits Landau levels in a magnetic field. Such motions are unrelated to polarizability and must be disentangled from the deformation energy on which the polarizabilities are defined. For this reason, most calculations have focused on neutral hadrons. For charged hadrons, what happens is that the two-point correlator does not develop single exponential behavior at large times.

In this work, we explore an alternative approach based on four-point functions in lattice QCD. Instead of background fields, electromagnetic currents couple to quark fields to induce interactions to all orders. It is a general approach that treats neutral and charged particles on equal footing, but particularly suited for charged particles. The trade-off is an increased computational demand of four-point functions. We know of two studies from a long time ago [1, 2], a recent calculation on the pion [3], and a preliminary one on the proton [4]. A reexamination of the formalism in Ref. [2] is recently carried out in Ref. [5] for both electric and magnetic polarizabilities of a charged pion and a proton.

Experimentally, polarizabilities are primarily studied by low-energy Compton scattering. Theoretically, a variety of methods have been employed to describe the physics involved, from quark confinement model [6], to NJL model [7], to linear sigma model [8], to dispersion relations [9, 10], to chiral perturbation theory (ChPT) [11, 12]. A recent review on pion polarizabilities can be found in Ref. [13].

2. Methodology

In Ref. [5], a formula is derived for electric polarizability of a charged pion,

$$\alpha_E^\pi = \frac{\alpha\langle r_E^2\rangle}{3m_\pi} + \lim_{\boldsymbol{q}\to 0}\frac{2\alpha a}{\boldsymbol{q}^2}\int_0^\infty dt\left[Q_{44}(\boldsymbol{q},t) - Q_{44}^{elas}(\boldsymbol{q},t)\right]. \tag{1}$$

Here $\alpha = 1/137$ is the fine structure constant and a the lattice spacing. The first term in the formula involves the charge radius and pion mass (we will refer to this term as the elastic contribution). The second term has the elastic contribution Q_{44}^{elas} subtracted from the total (we will refer to this term as the inelastic contribution). The formula will be used in discrete Euclidean spacetime but we keep the Euclidean time axis continuous for notational convenience. Special kinematics (called zero-momentum Breit frame) are employed in the formula to mimic low-energy Compton scattering.

The Q_{44} is defined as the $\mu = 4 = \nu$ component of the Fourier transforms,

$$Q_{\mu\nu}(\boldsymbol{q}, t_2, t_1) \equiv \sum_{\boldsymbol{x}_2, \boldsymbol{x}_1} e^{-i\boldsymbol{q}\cdot\boldsymbol{x}_2} e^{i\boldsymbol{q}\cdot\boldsymbol{x}_1} P_{\mu\nu}(\boldsymbol{x}_2, \boldsymbol{x}_1, t_3, t_2, t_1, t_0), \tag{2}$$

where $P_{\mu\nu}$ is a four-point function defined in position space (Ω denotes the vacuum),

$$P_{\mu\nu}(\boldsymbol{x}_2, \boldsymbol{x}_1, t_3, t_2, t_1, t_0) \equiv \frac{\sum_{\boldsymbol{x}_3, \boldsymbol{x}_0} \langle \Omega | \psi(x_3) : j^L_\mu(x_2) j^L_\nu(x_1) : \psi^\dagger(x_0) | \Omega \rangle}{\sum_{\boldsymbol{x}_3, \boldsymbol{x}_0} \langle \Omega | \psi(x_3) \psi^\dagger(x_0) | \Omega \rangle}. \tag{3}$$

Here ψ is the interpolating field of the pion and j^L_μ the lattice version of the electromagnetic current density. The two-point function in the denominator is for normalization. Normal ordering is used to include the required subtraction of vacuum expectation values (VEV) on the lattice. The sums over $\boldsymbol{x}_0$ and $\boldsymbol{x}_3$ enforce zero-momentum pions at the source (t_0) and sink (t_3). The two currents are inserted at t_1 and t_2 with two possibilities of time ordering implied in the normal ordering. At large time separations, it is dominated by the elastic contribution ($n = \pi$ term in the first sum), the form factor F_π can be determined from Q_{44} at large time separations,

$$Q^{elas}_{44}(\boldsymbol{q}, t) = \frac{(E_\pi + m_\pi)^2}{4 E_\pi m_\pi} F^2_\pi(\boldsymbol{q}^2)\, e^{-a(E_\pi - m_\pi)t}. \tag{4}$$

The charge radius $\langle r^2_E \rangle$ in the formula can then be extracted from F_π. Note that α_E has the expected physical unit of a^3 (fm^3) since $1/\boldsymbol{q}^2$ scales like a^2 and Q_{44} and t are dimensionless in our notation.

Wick contractions of quark-antiquark pairs in the unsubtracted part lead to topologically distinct quark-line diagrams shown in Fig. 1. In this work, we focus on the connected contributions. The

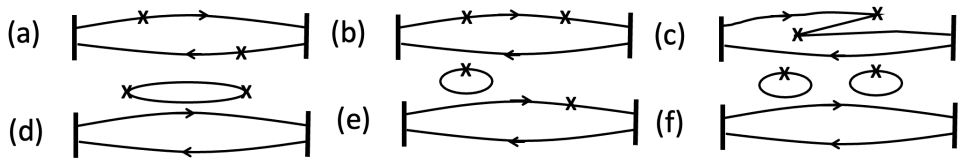

Figure 1: Quark-line diagrams of a four-point function contributing to polarizabilities of a meson. connected insertions (a), (b), (c); and disconnected insertions (d), (e), (f). The zero-momentum pion interpolating fields are represented by vertical bars (wall sources).

disconnected contributions are more challenging and are left for future work.

3. Simulation details and results

Having laid out the methodology and detailed the correlation functions, we now discuss how to numerically evaluate them in a Monte Carlo simulation in order to extract the polarizability. As a proof-of-principle test, we use quenched Wilson action with $\beta = 6.0$ and $\kappa = 0.1520,\ 0.1543,\ 0.1555,\ 0.1565$ on the lattice $24^3 \times 48$. The pion mass determined in our simulation is approximately 1100, 800, 600, and 370 MeV, respectively. We analyzed 500 configurations for $\kappa = 0.1520$ and 1000 configurations each for rest of the kappas. The scale of this action has been determined in Ref. [14], with inverse lattice spacing $1/a = 2.312$ GeV and kappa critical $\kappa_c = 0.15708$. Dirichlet (or open) boundary condition is imposed in the time direction, while

periodic boundary conditions are used in spatial dimensions. The pion source is placed at $t_0 = 7$ and sink at $t_3 = 42$ (time is labeled from 1 to 48). One current is inserted at a fixed time t_1, while the other current t_2 is free to vary. We use integers $\{n_x, n_y, n_z\}$ to label the discrete momentum on the lattice, and consider five different combinations $\{0,0,0\}$, $\{0,0,1\}$, $\{0,1,1\}$, $\{1,1,1\}$, $\{0,0,2\}$.

3.1 Four-point correlation functions

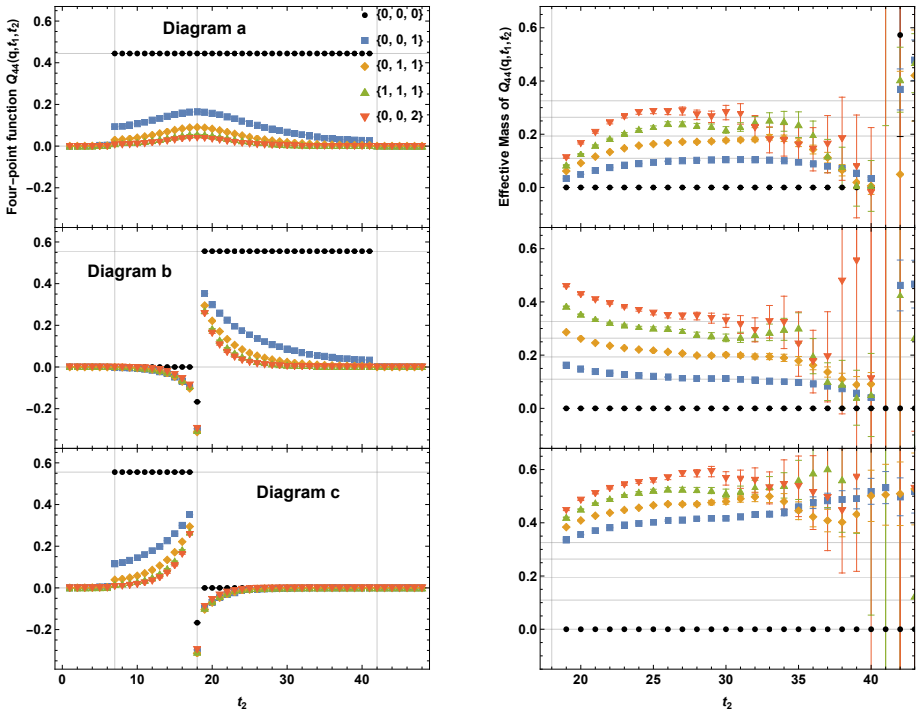

Figure 2: Normalized four-point functions (left panel) and their effective mass functions (right panel) from the connected diagrams as a function of current separation at $m_\pi = 600$ MeV. The $\boldsymbol{q} = 0$ results serve as a check of current conservation. The results for non-zero $\boldsymbol{q}$ between $t_2 = 18$ and $t_2 = 41$ will become the basis for our analysis. The vertical gridlines indicate the pion walls ($t_0 = 7$ and $t_3 = 42$) and the fixed current insertion ($t_1 = 18$). The horizontal gridlines in the effective mass functions indicate the value of $E_\pi - m_\pi$ where the continuum dispersion relation $E_\pi = \sqrt{\boldsymbol{q}^2 + m_\pi^2}$ is used.

Fig. 2 shows the raw normalized four-point functions Q_{44} at five different values of momentum $\boldsymbol{q}$ and at $m_\pi = 600$ MeV. For comparison purposes, all points in Q_{44} are displayed on the same linear scale. For the effective mass function $\ln Q_{44}(t)/Q_{44}(t+1)$, only points between the pion walls are displayed for clarity. The results are based on conserved currents and only the connected diagrams a, b and c. There are a number of interesting features in these plots. The results for $\boldsymbol{q} = 0$ confirms the current conservation property for fount-point functions,

$$\sum_{\boldsymbol{x}_2,\boldsymbol{x}_1} \langle\Omega|\psi(x)\, j_4^{(q_2,PS)}(x_2)\, j_4^{(q_1,PS)}(x_1)\, \psi^\dagger(0)|\Omega\rangle = q_1 q_2 \langle\Omega|\psi(x)\psi^\dagger(0)|\Omega\rangle. \tag{5}$$

In physical terms, the charge overlap at $\boldsymbol{q} = 0$ on the left-hand-side is effectively reconstructing the two-point function. Each charge density is spread over all spatial sites on the lattice. By summing

over $\boldsymbol{x}_1$ and $\boldsymbol{x}_2$ at zero momentum, we recover the total charge factor from each insertion, regardless of the time points of the insertions. Basically, for conserved current, we expect the ratio of four-point function to two-point function to approach the charge factor $q_u q_{\bar{d}} + q_d q_{\bar{u}} = 4/9$ for diagram a in the isospin limit, independent of current insertion points t_1 and t_2. For diagrams b and c, the factor is $q_u q_u + q_{\bar{d}} q_{\bar{d}} = 5/9$. Indeed, this is confirmed in all three diagrams (black dots). In diagram a, current conservation is limited between $t_2 = 7$ (on the pion wall source) and $t_2 = 41$ (one step inside the pion wall sink) because the two currents independently couple to two different quarks in this range. In diagram b, where they couple to the same quark, current conservation emerges only starting from $t_2 = 19$. In diagram c, it is limited between $t_2 = 7$ and $t_2 = 17$ because it is the Z-graph of b (different time-ordering). If diagrams b and c are added, then current conservation extends to the whole range, just like diagram a, except for the special point of $t_1 = t_2$ to be discussed below. Outside the regions of current conservation, the $\boldsymbol{q} = 0$ signal is exactly zero, while the $\boldsymbol{q} \neq 0$ signal gradually goes to zero towards the Dirichlet wall. There is a subtle issue with four-point functions. If the two currents couple to different quark lines ($q_1 \neq q_2$), the conservation is for all combinations of t_1 and t_2 between source and sink, including $t_1 = t_2$. If they couple to the same quark line ($q_1 = q_2$), the conservation is only true for $t_1 \neq t_2$. The point $t_1 = t_2$ introduces unwanted contact terms on the lattice. The issue is a lattice artifact; in the continuum, the contact interaction is regular and well-defined. Indeed we see that the special point of $t_1 = t_2$ is regular in diagram a, but gives irregular results in diagram b and c for all values of $\boldsymbol{q}$. We avoid this point in our analysis. Finally, the effective mass function of Q_{44} for diagram b approaches the value of $E_\pi - m_\pi$ at large separation times between t_1 and t_2. This is an indication that the four-point function for diagram b is dominated by the elastic contribution with a fall-off rate of $E_\pi - m_\pi$ according to Eq.(4). The same is true for diagram a, although deviations are slightly larger at higher momentum. The situation for diagram c, however, is completely different. The fall-off rates approach high above their respective $E_\pi - m_\pi$ values, suggesting they are dominated by inelastic contributions. In other words, the intermediate state is not a pion, but some four-quark state at higher mass and energy.

3.2 Elastic form factor

To account for possible violation of the continuum dispersion relation, we perform a fit to the functional form of Q_{44}^{elas} in Eq.(4), treating both $\{F_\pi, E_\pi\}$ as free parameters with m_π fixed at the measured values from two-point functions. After the form factor data are obtained, we fit them to the monopole form,

$$F_\pi(\boldsymbol{q}^2) = \frac{1}{1 + \boldsymbol{q}^2/m_V^2}, \tag{6}$$

which is the well-known vector meson dominance (VMD) commonly considered in pion form factor studies. The results are illustrated in Fig. 3. We see that the monopole form does not fit the data very well, especially at higher momentum and lower pion mass. For this reason, we also considered the z-expansion parametrization [15]

$$F_\pi(\boldsymbol{q}^2) = 1 + \sum_{k=1}^{k_{max}} a_k\, z^k, \text{ where } z \equiv \frac{\sqrt{t_{cut} - t} - \sqrt{t_{cut} - t_0}}{\sqrt{t_{cut} - t} + \sqrt{t_{cut} - t_0}} \text{ and } t = -\boldsymbol{q}^2,\ t_{cut} = 4m_\pi^2, \tag{7}$$

where a_k are free parameters and t_{cut} is the two-pion production threshold. We take $t_0 = 0$ so the form goes through $F_\pi(0) = 1$ by construction. Using this form, we can find a good fit with $k_{max} = 3$

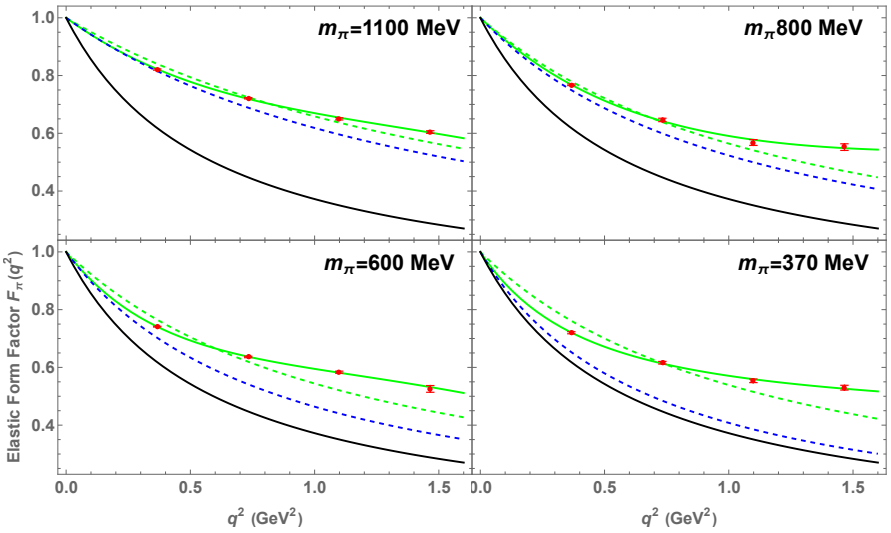

Figure 3: Pion elastic form factors extracted from four-point functions. The red data points are the measured values. The green solid line is a fit to the z-expansion in Eq. (7). The green dashed line is a fit to the monopole form in Eq. (6). The blue dashed line is the same monopole form plotted with the measured rho mass, and the black solid line with the physical rho mass.

in all cases. For comparison, we also plot the monopole function with the measured rho mass m_ρ and the physical rho mass of $m_\rho^{phys} = 0.77$ GeV. We observe significant differences between the fitted monopole form (m_V) and the VMD form (m_ρ). The difference grows with increasing momentum and decreasing pion mass. Similar behavior has been observed in previous studies [16, 17]. Once the functional form of form factor is determined, the charge radius is obtained by

$$\langle r_E^2 \rangle = -6 \frac{dF_\pi(\boldsymbol{q}^2)}{d\boldsymbol{q}^2}\Big|_{\boldsymbol{q}^2 \to 0}. \tag{8}$$

Their values in physical units are put in Table 1.

Table 1: Summary of results in physical units from two-point and four-point functions. Two sets of results are given for charge radius: one from z-expansion fits to the form factor, one from monopole fits. The average of the two is used to determine elastic α_E. The total α_E is smoothly extrapolated to the physical point. This extrapolated value, in conjunction with the elastic α_E derived from charge radius and pion mass given by PDG, yields the prediction for the inelastic α_E at the physical point. All α_E values are in units of 10^{-4} fm^3.

	κ=0.1520	κ=0.1543	κ=0.1555	κ=0.1565	physical point
m_π (MeV)	1104.7 ± 1.2	795.0 ± 1.1	596.8 ± 1.4	367.7 ± 2.2	138.000
m_ρ (MeV)	1273.1 ± 2.5	1047.3 ± 3.4	930. ± 7.	830. ± 17.	770.000
$\langle r_E^2 \rangle$ (fm^2	0.1329 ± 0.0018	0.187 ± 0.004	0.2266 ± 0.0025	0.252 ± 0.008	0.434 ± 0.004
α_E elastic	0.577 ± 0.008	1.129 ± 0.023	1.820 ± 0.021	3.29 ± 0.11	15.08 ± 0.13
α_E inelastic	−0.304 ± 0.006	−0.605 ± 0.007	−0.846 ± 0.005	−1.148 ± 0.010	−11.84 ± 0.29
α_E total	0.273 ± 0.010	0.523 ± 0.023	0.975 ± 0.021	2.14 ± 0.11	3.24 ± 0.31

3.3 Electric polarizability

In Fig. 4 we show separately the total contribution Q_{44} (from all three diagrams) and Q_{44}^{elas} as a function of current separation $t = t_2 - t_1$. W use $m_\pi = 600$ MeV as an example; the graphs at the other pion masses look similar. Note that although Q_{44}^{elas} is obtained in the large time region, the subtraction is done in the whole region according to the functional form in Eq.(4). Most of the contribution is in the small time region where inelastic contributions are significant. We observe that Q_{44}^{elas} is consistently larger than Q_{44}, suggesting that the inelastic term in the formula is negative. The time integral is simply the negative of the shaded area between the two curves. One detail to notice is that the curves include the $t = 0$ point which has unphysical contributions in Q_{44} as mentioned earlier. We would normally avoid this point and only start the integral from $t = 1$. However, as one can see, the chunk of area between $t = 0$ and $t = 1$ is the largest piece in the integral. To include this contribution, we linearly extrapolated the Q_{44} term back to $t = 0$ using the two points at $t = 1$ and $t = 2$. This will incur a systematic effect on the order of $O(a^2)$ since the error itself is order of $O(a)$. As the continuum limit is approached, the systematic effect will vanish (the chunk will shrink to zero). There is no issue to include this point in Q_{44}^{elas} using its functional form. The entire second term (prefactor and time integral) is a function of momentum. Since α_E is a static property, we extrapolate it to $\boldsymbol{q}^2 = 0$ smoothly. To assess the systematic effect of this extrapolation, we consider two fitting forms, one is $a + bx + cx^2$ ($x = \boldsymbol{q}^2$) using all data points, the other a simple linear extrapolation using the two lowest points. The results are shown in Fig. 4 for all pion masses.

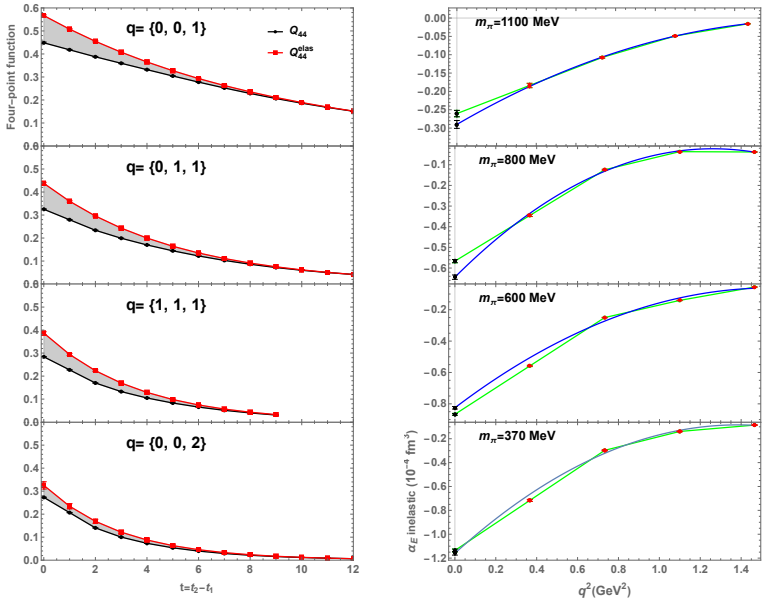

Figure 4: Left: Total Q_{44} and elastic Q_{44}^{elas} at different values of $\boldsymbol{q}$ at $m_\pi = 600$ MeV. The shaded area, $\int dt\left[Q_{44}(\boldsymbol{q},t) - Q_{44}^{elas}(\boldsymbol{q},t)\right]$, is the signal contributing to polarizability. Right: Extrapolation of the second term (inelastic) in Eq. (1) to $\boldsymbol{q}^2 = 0$ in physical units. The red points are based on the shaded areas in Fig. 4. The blue curve is a quadratic extrapolation using all points. The green curve is a linear extrapolation based on the two smallest $\boldsymbol{q}^2$ values with straight lines connecting all the points. The black points indicate the extrapolated values contributing to α_E.

One observes a difference between the two that decreases with decreasing pion mass. The difference in the extrapolation is a systematic effect in the analysis. We will use the average of the two values to determine α_E.

We summarize all of the results measured in this study in Table 1. We use the average of monopole and z-expansion to determine the elastic α_E. To see how the trend continues in pion mass, we include the physical point in the following way. We take the total values for α_E and perform a smooth extrapolation to the physical point using the $a + bm_\pi + cm_\pi^2$ form. The extrapolated value $\alpha_E = 3.24 \pm 0.31$ can be compared to known values for charged pion α_E. PDG [18] quotes a value $\alpha_E = 2.0 \pm 0.6 \pm 0.7$ from experiment with large uncertainties. ChPT [19] gives $\alpha_E = 2.8$. Our values are comparable. We also attempted to extrapolate the total α_E using the $1/m_\pi$ form expected from ChPT. This form does not fit our data well which is not surprising since some of our pion masses lie beyond the region of validity for ChPT. Chiral extrapolation is an open issue that warrants further study when the calculation is extended to smaller pion masses.

To get a sense of individual contributions at the physical point, we take the PDG value $\langle r_E^2 \rangle = 0.435(4)$ fm^2 and physical m_π to arrive at the elastic α_E value of 15.08(13). Then the inelastic value of $\alpha_E = -11.84(29)$ can be inferred from the total and the elastic. We should mention that our value is consistent with the inelastic contribution obtained in another lattice study [3] near physical pion mass. It employs a formula derived from a different method but has a similar structure.

In any event, a physical picture starts to emerge from our results. In the approach to the physical point, the elastic contribution grows positive strongly; at the same time the inelastic contribution grows negative strongly; the total is relatively small and positive and has a mild pion mass dependence.

4. Conclusions and acknowledgements

We investigated the feasibility of using four-point functions in lattice QCD to extract charged pion electric polarizability. The approach is based on low-energy Compton scattering tensor constructed with quark and gluon fields in Euclidean spacetime [5]. The central object is the formula given in Eq.(1) which consists of two terms. One is an elastic contribution involving charge radius $\langle r_E^2 \rangle$ and pion mass. The other an inelastic contribution in the form of a subtracted time integral. In addition to four-point functions, it requires two-point functions for pion mass and normalization, but not three-point functions. The elastic contribution can be obtained from the same four-point function in the elastic limit. The simulation demonstrates that the four-point function methodology can be a viable alternative to the background method for polarizabilities of charged hadrons. We caution that the picture is subject to a number of systematic effects at this stage, such as the quenched approximation, finite-volume effects, and disconnected loops. Aside from these effects, the largest source of uncertainty in the present analysis is in charge radius determination. We observe significant differences between monopole and z-expansion. Our final results are based on the average of the two. Although the uncertainty does not alter the picture qualitatively, it matters for quantitative comparisons.

The analysis procedure used to determine α_E in Eq.(1) involves multiple steps which we summarize here. 1) Fit Type 1 two-point function to obtain m_π (and m_ρ). 2) Fit four-point function $Q_{44}^{(ab)}$ from diagrams a and b to Q_{44}^{elas} at large times for elastic form factor F_π. 3) Fit F_π data to a

functional form (monopole or z-expansion), then extract charge radius $\langle r_E^2 \rangle$. 4) Perform subtraction $Q_{44}^{(abc)}(\boldsymbol{q}) - Q_{44}^{elas}(\boldsymbol{q})$ at small times using all three diagrams a,b,c. Do the time integration. Extrapolate back to $t = 0$ to include the missing chunk due to contact terms. 5) Extrapolate the inelastic term to $\boldsymbol{q}^2 = 0$ to obtain the static limit, then assemble everything in physical units for α_E. 6) Extrapolate the total α_E in pion mass to the physical point.

Going forward, the investigation can proceed in multiple directions. First, the quenched approximation should be removed by employing dynamical fermions. Work is underway to use our collection of two-flavor nHYP-clover ensembles [20] which have been successfully used in a number of physics projects. They have smaller pion masses (about 315 MeV and 227 MeV) that can be used to check the expected chiral behavior and facilitate a chiral extrapolation study. The elongated geometries in these ensembles offer a cost-effective way of studying finite-volume effects and reaching smaller $\boldsymbol{q}$ values. It would be interesting to see how the charge radius is affected by the change of action. Second, a simulation of charged pion magnetic polarizability (β_M) is straightforward. The formula has been derived in Ref. [5]. One just needs to replace Q_{44} with Q_{11} in the formalism. It would be interesting to check the well-known prediction $\alpha_E + \beta_M \approx 0$ from ChPT. Third, the disconnected contributions should be included. This is a challenging task. Although disconnected loops generally give smaller contributions than connected ones, they must be dealt with for a complete picture from lattice QCD. Fourth, the methodology can be equally applied to neutral particles (for example π^0 and the neutron). The advantage it offers over the background field method is the natural treatment of disconnected loops (or sea quarks) [21, 22]. Our ultimate target is the proton for which a formula is also available [5]. A first-principles-based calculation of its polarizabilities will be a valuable addition to the Compton scattering effort in nuclear physics.

This work was supported in part by U.S. Department of Energy under Grant No. DE-FG02-95ER40907 (FL, AA) and UK Research and Innovation grant MR/S015418/1 (CC). The calculations are carried out at DOE-sponsored NERSC. AA would like to acknowledge support from University of Maryland. WW would like to acknowledge support from the Baylor College of Arts and Sciences SRA program.

References

[1] M. Burkardt, J. Grandy and J. Negele, *Calculation and interpretation of hadron correlation functions in lattice qcd*, *Annals of Physics* **238** (1995) 441.

[2] W. Wilcox, *Lattice charge overlap. 2: Aspects of charged pion polarizability*, *Annals Phys.* **255** (1997) 60 [hep-lat/9606019].

[3] X. Feng, T. Izubuchi, L. Jin and M. Golterman, *Pion electric polarizabilities from lattice QCD*, *PoS* **LATTICE2021** (2022) 362 [2201.01396].

[4] X. Wang, X. Feng and L. Jin, *Lattice QCD calculation of the proton electromagnetic polarizability*, *LATTICE2021 proceedings* (2022) .

[5] W. Wilcox and F.X. Lee, *Towards charged hadron polarizabilities from four-point functions in lattice QCD*, *Phys. Rev. D* **104** (2021) 034506 [2106.02557].

[6] M.A. Ivanov and T. Mizutani, *Pion and kaon polarizabilities in the quark confinement model*, *Phys. Rev. D* **45** (1992) 1580.

[7] V. Bernard and D. Vautherin, *Electromagnetic polarizabilities of pseudoscalar goldstone bosons*, *Phys. Rev. D* **40** (1989) 1615.

[8] V. Bernard, B. Hiller and W. Weise, *Pion electromagnetic polarizability and chiral models*, *Physics Letters B* **205** (1988) 16.

[9] B. Pasquini, D. Drechsel and S. Scherer, *Reply to "comment on 'polarizability of the pion: No conflict between dispersion theory and chiral perturbation theory"'*, *Phys. Rev. C* **81** (2010) 029802.

[10] L.V. Fil'kov and V.L. Kashevarov, *Dipole polarizabilities of charged pions*, *Physics of Particles and Nuclei* **48** (2017) 117.

[11] M. Moinester and S. Scherer, *Compton Scattering off Pions and Electromagnetic Polarizabilities*, *Int. J. Mod. Phys. A* **34** (2019) 1930008 [1905.05640].

[12] F. Hagelstein, *Nucleon Polarizabilities and Compton Scattering as a Playground for Chiral Perturbation Theory*, *Symmetry* **12** (2020) 1407 [2006.16124].

[13] M. Moinester, *Pion Polarizability 2022 Status Report*, 5, 2022 [2205.09954].

[14] S. Cabasino, F. Marzano, J. Pech, F. Rapuano, R. Sarno, G. Todesco et al., *beta=6.0 quenched wilson fermions*, *Physics Letters B* **258** (1991) 195.

[15] G. Lee, J.R. Arrington and R.J. Hill, *Extraction of the proton radius from electron-proton scattering data*, *Physical Review D* **92** (2015) .

[16] T. Draper, R.M. Woloshyn, W. Wilcox and K.-F. Liu, *The Pion Form-factor in Lattice QCD*, *Nucl. Phys. B* **318** (1989) 319.

[17] J. van der Heide, J.H. Koch and E. Laermann, *Pion structure from improved lattice QCD: Form factor and charge radius at low masses*, *Physical Review D* **69** (2004) .

[18] Particle Data Group collaboration, *Review of Particle Physics*, *PTEP* **2022** (2022) 083C01.

[19] B.R. Holstein and S. Scherer, *Hadron polarizabilities*, *Annual Review of Nuclear and Particle Science* **64** (2014) 51.

[20] H. Niyazi, A. Alexandru, F.X. Lee and R. Brett, *Setting the scale for nHYP fermions with the Lüscher-Weisz gauge action*, *Phys. Rev. D* **102** (2020) 094506 [2008.13022].

[21] W. Freeman, A. Alexandru, F.X. Lee and M. Lujan, *Update on the Sea Contributions to Hadron Electric Polarizabilities through Reweighting*, in *31st International Symposium on Lattice Field Theory*, 10, 2013 [1310.4426].

[22] W. Freeman, A. Alexandru, M. Lujan and F.X. Lee, *Sea quark contributions to the electric polarizability of hadrons*, *Phys. Rev. D* **90** (2014) 054507 [1407.2687].